Open Access Journal

Journal of Power Technologies 95 (1) (2015) 54–66

journal homepage:papers.itc.pw.edu.pl

Low temperature-ethanol steam reforming over Ni-based catalysts supported on CeO_2

Vincenzo Palma[a], Filomena Castaldo[*,a], Concetta Ruocco[a], Paolo Ciambelli[a], Gaetano Iaquaniello[b]

[a]*Dipartimento di Ingegneria Industriale, Universita di Salerno*
Via Giovanni Paolo II, 84084 (SA), Italy
[b]*Tecnimont KT S.p.A.*
Viale Castello della Magliana 75, 00148 Roma, Italy

Abstract

Recent research has been focused on methods to produce hydrogen. There is growing interest in the properties of hydrogen as an energy carrier and the prospects look good for hydrogen use in fuel cell applications, especially when production processes involve clean, renewable sources.
Although natural gas steam reforming is the most common way to obtain hydrogen, ethanol steam reforming (ESR) may reduce the dependence on fossil fuels and cut harmful emissions.
The ESR reaction is promoted at high temperatures, being strongly endothermic, but in some cases it can be performed at low temperatures, using this process as a pre-reforming step before conventional methane steam reforming (MSR). The low temperature range could reduce: the thermal duty, costs and CO formation, making the produced hydrogen capable of being fed into a fuel cell.
The performances of Ni-based catalysts for ethanol steam reforming in a low temperature range (LT-ESR) were evaluated. In particular, the activity of bimetallic samples, prepared by impregnation and coprecipitation, was monitored in both diluted and concentrated feed stream conditions. By comparing bimetallic catalysts with monometallic ones prepared at different Pt or Ni loadings, it was possible to identify the most suitable sample. 3%wtPt / 10wt%Ni / CeO_2 obtained by impregnation achieved the highest performances in terms of both H_2 yield and durability, allowing perfect agreement with thermodynamic data. However, during stability tests, reaction plugging phenomena occurred. By changing the water-to-ethanol molar ratio from 3 to 6, a considerable increase in durability was observed. The investigation of exhaust catalysts through various characterization techniques was helpful for studying in detail possible sintering or deactivation occurrence.

Keywords: Bimetallic catalysts, Bio-ethanol, Hydrogen, Steam reforming

1. Introduction

Hydrogen will play a key role in the trend toward harnessing sustainable energy sources. The demand for hydrogen is continually increasing due to its use as an energy source in hydrogen fuel cells. Hydrogen production from various primary energy sources such as fossil fuels and biomass could prove to be a very important technology for meeting future energy demand. At present, regardless of the feedstock, hydrogen is mainly produced through catalytic steam reforming processes. The reactions are strongly endothermic, consequently they usually take place in a high temperature range of 700...900°C. Thus a large amount of energy is consumed, which becomes a great obstacle in on-site hydrogen production such as fuel cell application.

High temperature processes require a lengthy start-up time for heating the catalyst bed and a heat-exchanger for achieving higher energy efficiency. However, small commercial technologies require a quick start-up and simple processes, so the use of high temperatures causes serious problems [1–3]. Therefore, a catalytic process working at lower temperatures is desired, and high energy efficiency cou-

[*]Corresponding author
Email address: fcastaldo@unisa.it (Filomena Castaldo[*,])

pled with fast start-up features is the optimal compromise. To date, many processes have been proposed for low temperature hydrogen production, including oxidative reactions like partial oxidation of methane / hydrocarbons to produce syngas, autothermal reforming, and oxidative steam reforming (oxyreforming). Some researchers have investigated autothermal reforming and partial oxidation of methane / hydrocarbons to produce synthesis gas at lower temperatures than steam reforming of methane, but their use of exothermic reactions (oxidation) decreases the fuel's calorific value [4–6].

Lowering the temperature may reduce energy consumption and the cost associated with the material of the reformer. However, it will also affect conversion and catalytic activity. Therefore, a catalyst with high catalytic activity at lower reaction temperature is required in a realistic system.

Considering that MSR significantly impacts the environment, through the use of a non-renewable source and emissions of toxic gases, clean and renewable raw materials have been proposed for the steam reforming reaction [7–10]. As a mature technology related to reformation of hydrocarbons already exists, the implementation of reformation processes involving other substrates, such as alcohols, seems highly realistic [11].

Recently, industrial research has focused on ethanol, which appears a good candidate for several reasons: it is renewable, increasingly available, easy to transport, biodegradable, and low in toxicity; moreover, it easily decomposes in the presence of water to generate a hydrogen-rich mixture and is free of catalyst poisons such as sulfur. Furthermore, a bio-ethanol to hydrogen system has two significant advantages: (i) it is nearly CO_2 neutral, since the carbon dioxide produced in the process is consumed for biomass growth, offering a nearly closed carbon loop; (ii) bio-ethanol, i.e. ethanol in aqueous solution, obtained through the biomass fermentation can be used directly: in fact, since steam is necessary for the reforming reaction, an expensive step for the separation of water is not required [12–14].

Ethanol steam reforming (ESR) is a catalytic and endothermic reaction (1).

$$C_2H_5OH+3H_2O \Leftrightarrow 6H_2+2CO_2 \quad [\Delta H_{298K} = -174\,kJ/mol] \tag{1}$$

There are other reaction pathways, mostly undesired, that could occur in parallel or in series. Some of them involve C_2H_5OH dehydration to ethylene (C_2H_4) and water, followed by polymerization of C_2H_4 to form coke, C_2H_5OH decomposition or cracking to CH_4, followed by steam reforming, C_2H_5OH dehydrogenation to acetaldehyde (C_2H_4O), followed by decarbonylation or steam reforming of C_2H_4O, C_2H_5OH decomposition into acetone (CH_3COCH_3), followed by steam reforming [15–17].

Various authors have tried to perform a thermodynamic analysis of the ethanol steam reforming reaction, concluding that high temperature, together with a high water-to-ethanol molar ratio and low pressure are necessary to promote selectivity towards hydrogen instead of by-products formation [18–20].

In order to feed the hydrogen produced through steam reforming to a fuel cell, some downstream purification processes are necessary, in particular the CO-WGS reaction is needed to remove the carbon monoxide, which is harmful to fuel cell anodes. Since it is exothermic, the WGS reaction is promoted at low temperatures. Moreover, high temperature ESR can suffer from thermal inefficiencies. As a result, a low temperature range has also been proposed [21, 22]. When carried out at temperatures lower than 600°C, ESR can provide a hydrogen-rich gas and it is also possible to reduce the overall thermal duty, enhancing plant compactness and lowering the capital costs.

LT-ESR is characterized by a high selectivity toward the formation of coke precursors, responsible for faster catalyst deactivation. As a consequence, the choice of catalyst is crucial in LT-ESR in order to obtain, at low temperature, a gas stream rich in CH_4 and H_2 with low CO content, and also to inhibit coke formation, ensuring high stability for the system [23, 24].

Recent literature deals with the steam reforming of ethanol on various catalytic systems, mainly supported on CeO_2: its oxygen storage / transport capacity and high oxygen mobility [25–27] render this material very interesting for steam reforming reactions to give stability to the final catalyst, oxidizing possible coke deposits.

Noble metals (Au, Pd, Pt, Rh, Ru, Ir) as active species were found to be very active in steam reforming and WGS reactions [28–30]. For reasons of cost, non-noble metals have also been proposed [27–33], taking advantage of their ability to break C-C bonds.

Nickel-based catalysts employing stable inert oxide supports, such as Al_2O_3 and MgO, are still commercially used due to the reduced cost, despite serious problems of coke formation and relatively low activity compared to noble metals. Recently, catalysts containing more than one active species (e.g. Cu-Ni, Co-Al, Cu-Zn-Al, Pt-Ni, Pd-Ag-Ni, Ni-Co, Pt-Co) have also been investigated because of their significantly different catalytic properties with respect to either of the parent metals [34–37]. Bimetal-

lic catalysts may sometimes exhibit superior activity, selectivity and deactivation resistance compared to those of the corresponding monometallic ones. Enrichment of Ni-based catalysts formulations by a very small amount of noble metal can result in an inexpensive bimetallic supported system assuring both high activity and higher coking resistance. It has been reported that the introduction of a small amount of Pt into Ni / ZSM-5 led to a significant improvement in activity and stability of the catalyst, which was attributed to increased Ni metallic dispersion caused by the intimate contact between Ni and Pt at Ni loading of 6 wt.% [38]. Also, by adding platinum to other non-noble metals, such as Co, sensible gains can be achieved. In fact, it was found that in the case of bimetallic Ni- or Co-based samples, enhanced catalytic performances are possible even at an intermediate Pt load, lower than the amount of platinum necessary in the monometallic catalyst to obtain satisfactory activity and durability [39].
In the present work, we examined hydrogen production by LT-ESR over Ni- based catalysts. In order to the select the best catalytic formulation, monometallic and bimetallic samples performances were compared, also studying the effect of Pt addition. The properties of the catalysts, prepared by two different techniques (impregnation and coprecipitation), were highlighted through a series of characterization techniques. Moreover, the influence of reaction temperature, space velocity and feeding conditions on activity and selectivities was investigated. After preliminary screening, the stability of the most interesting catalyst was evaluated, with the intention being to examine the possible coke formation tendency.

2. Experimental methods

2.1. Preparation of catalysts

The bimetallic catalysts were prepared by wet impregnation and coprecipitation methods. In both cases, before preparation, the support, commercially available CeO_2 (Aldrich, BET surface area of 80 m^2 / g), was calcined in air at 600°C for 3 h (dT / dt=10°C / min) in a muffle furnace.
All chemicals used were HPLC grade obtained from Aldrich.
The impregnated samples were obtained by dispersing the calcined support in an aqueous solution of the active metal precursors (0.1 M for Ni impregnation and 0.01 for Pt one), the nickel acetate ($C_4H_6O_4Ni{\cdot}4H_2O$) or the platinum chloride ($PtCl_4$).
The impregnation procedure was carried out for 3 hours at 80°C and then drying overnight at 120°C and calcination, carried out in the same conditions of the support, occurred. Two following impregnations were performed and the amount of precursor was selected in order to obtain the desired metal loads, equal to 3wt% for the noble metal and to 10wt% for the non-noble metal. These values were optimized previously [39].
The coprecipitation technique starts by adding a NaOH 2 M solution to the aqueous solution of metal salts. The resulting precipitate was centrifuged, washed, dried overnight at 120°C and finally calcined.
The performance of a monometallic Ni / CeO_2 catalyst was compared with the behavior of bimetallic samples, based on Ni with an ascending amount of noble metal. The monometallic Ni-, Co- and Pt-based samples have been previously studied in detail [39], preparing them using the impregnation method and characterizing through different techniques. It was found that the optimal metal load was equal to 10wt% for a non-noble metal and at least 5wt% for platinum, the latter amount being required to increase the stability and CH_4 selectivity. The experimental tests results also showed that the addition of 10% wt of a non-noble metal makes it possible to achieve excellent performance even at the intermediate Pt load (1...3wt%).
In this paper, the monometallic Pt- and Ni-based catalysts, supported on CeO_2, were considered as a reference for the CeO_2-supported bimetallic samples, containing both Pt and Ni, which were studied in detail. The catalysts were obtained through coprecipitation and impregnation; in the latter case, the order of deposition of metals was also investigated. The impregnated bimetallic samples were denoted Pt / Ni or Ni / Pt, depending on the order of impregnation, while the coprecipitated ones were denoted Pt-Ni; the metals' names were preceded by the metal load (e.g. 1Pt / 10Ni is a catalyst prepared by impregnation and containing 1wt% of Pt and 10wt% of Ni). The samples were properly characterized and the results were compared with the properties of the monometallic ones, previously investigated. The catalytic performances in the LT-ESR were evaluated in terms of activity, selectivity and stability, in both diluted and concentrated conditions.

2.2. Characterization of catalysts

The catalysts were characterized by EDXRF analysis, N_2 adsorption at -196°C, X-Ray Diffraction (XRD), Temperature Programmed Reduction (TPR), Thermogravimetric analysis-Mass Spectrometer (TG-MS), Micro Raman Spectroscopy and TEM analysis.
Chemical analysis was performed by Energy Dispersive X-Ray Fluorescence (EDXRF) analysis (Thermo-Scientific QUANT'X).
N_2 adsorption at -196°C was carried out through a Costech adsorption equipment, SORPTOMETER 1040 "Kelvin"

by Costech Analytical Technologies. Each catalyst underwent pre-treatment at 150°C for 1h in He flow to remove possible moisture from the catalyst surface, followed by specific surface area measurement using the B.E.T. method.
XRD was performed in a D-max-RAPID X-ray microdiffractometer, with a cylindrical imaging plate detector, which with Cu-Kα radiation enables the collecting of diffraction data from 0 to 204° (2ϑ) horizontally and from -45 to 45° (2ϑ) vertically. The incident beam collimators enable different spot sizes to be projected onto the sample. The equipment operated at 40 kV and 20 mA.
The average oxides crystallite sizes were calculated using the Scherrer formula:

$$d = \frac{k\lambda}{\beta \cos\theta} \tag{2}$$

where:

- k is the dimensionless shape factor (0.9);
- λ is the wave length (typically 1.54 $\AA$);
- β is the width at half height of the maximum intensity (also known as FWHM: full width at half maximum) in radiant;
- θ is the diffraction angle.

TPR measurements were performed in the laboratory apparatus for ethanol steam reforming. Fresh catalysts, before every ESR test, were reduced in situ at 600°C for 1 h at 10°C / min heating rate under 1,000 cm^3 / min flow rate of a gas mixture containing 5 vol% of H_2 in N_2.
TG analysis were carried out in a thermogravimetric analyzer Q600, TA Instrument (at 800°C at 10°C / min in air), coupled with a Mass Spectrometer (MS).
The Raman spectra were produced with a Dispersive MicroRaman (Invia, Renishaw), equipped with 785 nm diode-laser, in the range 100...2,500 cm^{-1} Raman shift.
TEM observations were performed with a FEI Tecnai F20 equipped with an EDX spectrometer.
All the characterization tests were carried out at the Department of Industrial Engineering of the University of Salerno, except for the TEM analysis, which was performed at the Department of Earth Science "Ardito Desio" of the University of Milan.

2.3. Lab-scale apparatus: description & procedure

The catalytic tests were carried out on the catalyst, after the TPR measurements, using laboratory apparatus (Fig. 1) which can be easily modified depending on the desired experiment.

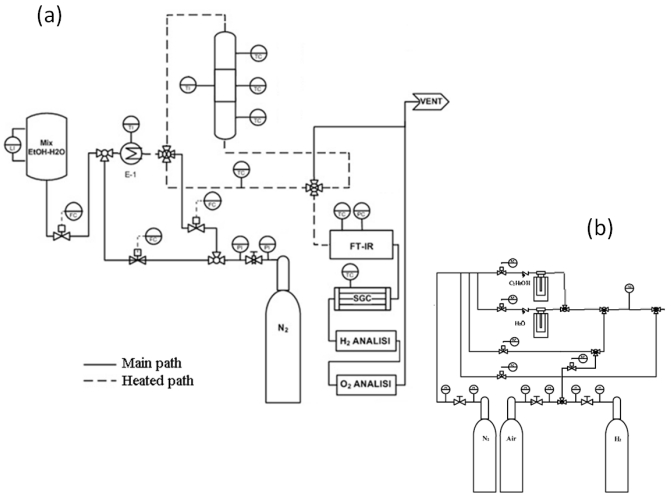

Figure 1: (a) Experimental set up apparatus; (b) Feed section for diluted tests

All the gas pipes (1 / 4" OD) are of Teflon, while the connections are made with Swagelok union and two, three and four way Nupro valves; all the gas comes from SOL S.p.A with a purity degree of 99.999%.
The bio-ethanol feed stream is simulated by preparing a solution of bidistilled water and pure ethanol. The preliminary activity tests were undertaken using a diluted feed stream, with the following feed gas composition: 0.5 vol% EtOH / 1.5 vol% H_2O / 98 vol% N_2. In this case, the reactants were fed through saturation of a nitrogen flow at fixed temperature (Fig. 1b). Therefore a water-to-ethanol ratio, defined as $r.a. = \frac{moles_{H_2O}}{moles_{C_2H_5OH}}$, which was equal to 3 and a dilution ratio, defined as $r.d. = \frac{moles_{N_2}}{moles_{C_2H_5OH} + moles_{H_2O}}$, which was equal to 49 were employed.
In reality, the raw bio-ethanol stream contains up to 12%wt of ethanol, which is about 5vol% of ethanol in the gas phase. Thus, after preliminary screening in diluted conditions, more concentrated feed mixtures were used, with r.d. values of 4, 1.5 and 0.67, equivalent to 5, 10 and 15vol% of ethanol in the feed stream. In these conditions, it was indispensable for the feed equipment to properly vaporize the liquid fuel. The liquid ethanol / water mixture, prepared depending on the desired molar ratio between the two substances, is stored in a tank and sent to the vaporization section after premixing with a N_2 dilution stream, and fed through a Brooks 5850 mass flow controller (MFC). To feed an accurately controlled flow, a Coriolis controller is used (Quantim by Brooks).
In both diluted and concentrated conditions, a water-to-ethanol molar ratio corresponding to the stoichiometric ratio was used. From the thermodynamic analysis, this

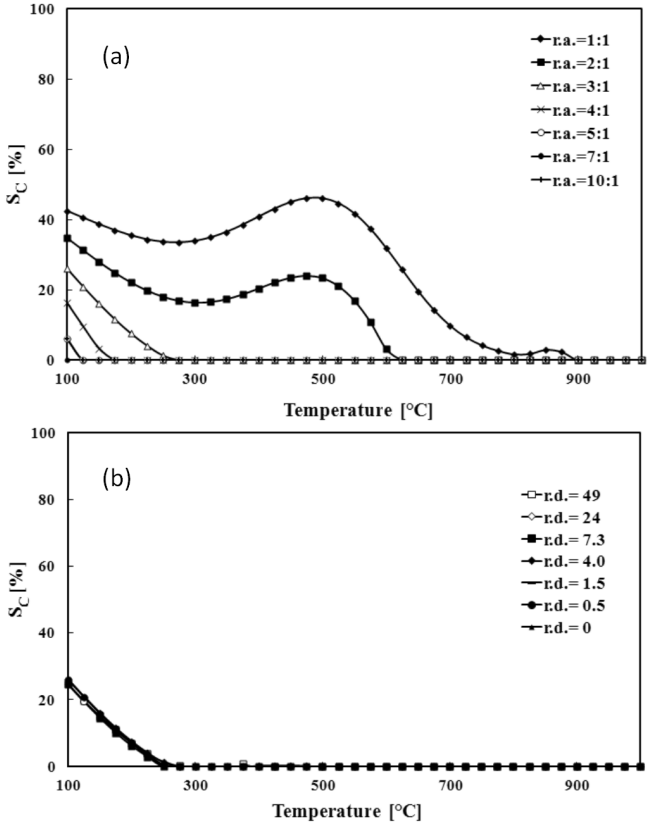

Figure 2: Coke selectivity (S_c) as a function of temperature at different water-to-ethanol molar ratios (a) and dilution ratios (b) from thermodynamic calculations

was found to be the minimum value to avoid coke formation, as reported in Fig. 2a, in which it is possible to observe coke selectivity as a function of temperature and r.a.. In contrast, carbonaceous species selectivity is not significantly affected by r.d. variations (Fig. 2b).

The reaction section is characterized by a three zone electric oven in which is placed a tubular stainless steel (AISI-310) reactor (18 mm i.d.). The catalytic bed is located in its annular section and the powder catalyst (180...355 mm) is typically sandwiched between quartz flakes of same dimensions of the reactor. The temperature in the oven is controlled by three temperature programmer-controllers (TLK 43 by Tecnologic) connected to three K-type thermocouples located inside the oven while the temperature of the catalytic bed is measured through three other K-type thermocouples that are placed at the inlet, the middle and the outlet of the catalytic bed. A differential pressure sensor controls the pressure drops through the catalytic bed.

The products at the reactor outlet can be detected through an online FT-IR multigas analyzer, able to simultaneously analyze and display more than 30 gases, in addition to noble gases such as xenon and argon, and homomolecular diatomic molecules such as O_2, N_2 and H_2. The H_2 and O_2 concentrations were measured respectively by a CALDOS 27 thermoconductivity analyzer and a MAGNOS 206 paramagnetic analyzer. ABB continuous analyzers were also supplied with a sample gas conditioning system. The analyzers were connected via ethernet to the PC by the AO-OPC server, a standard software interface to the AO 2000 series ABB gas analyzers.

To avoid water condensation, the whole connection from the feed section to the FT-IR gas analyzer was heated by heating tapes controlled by a K-type thermocouple connected to a temperature programmer controller: TLK 43 by Tecnologic.

The gas cell used in diluted conditions was characterized by an optical path length of 2 m while, for concentrated conditions tests, a new cell with an optical path length of 12 cm was designed in order to avoid saturation phenomena.

Catalytic tests in diluted and concentrated conditions were performed at Q_{tot}=1000 Ncm^3 / min and GHSV=15,000 h^{-1}; catalyst performances were evaluated through ethanol conversion, hydrogen yield and products selectivity:

$$X_{EtOH} = \frac{(moles_{EtOH,in} - moles_{EtOH,out})}{moles_{EtOH,in}} \cdot 100$$

$$Y_{H_2} = \frac{(moles_{H2,out}/6)}{moles_{EtOH,in}} \cdot 100$$

$$S_P = \frac{moles_{product,out}}{(\nu) * (moles_{EtOH,in} - moles_{EtOH,out})} \cdot 100$$

where

- P...-product(CH_4, H_2O, CO, CO_2)
- n...-stoichiometric ratio between the reaction product and ethanol.

3. Results and discussion

3.1. Characterization results

The characterizations of the bimetallic catalysts are discussed in detail. From the SSA measurements, reported in Table 1, a clear reduction of specific area with respect to CeO_2 alone was observed. The support calcination step, which foregoes impregnation, induced the first SSA lowering from 80 to 60 m^2 / g; also the deposition of metals on CeO_2 caused a considerable decrease in the specific surface area, probably due to the crystallites rearrangement and the metals-support interaction during preparation and calcination step [40].

Table 1: List of catalysts and support and results of ICP analysis, SSA evaluation tests and crystallites dimension calculations

Catalyst	Metal content by ICP analysis		SSA, m^2 / g	d_{CeO2}, nm	d_{NiO}, nm
	Pt	Ni			
3Pt / 10Ni	2.8	9.8	42	23	21
10Ni / 3Pt	2.7	10.8	39	26	18
3Pt-10Ni	3.2	10.9	41	6	21

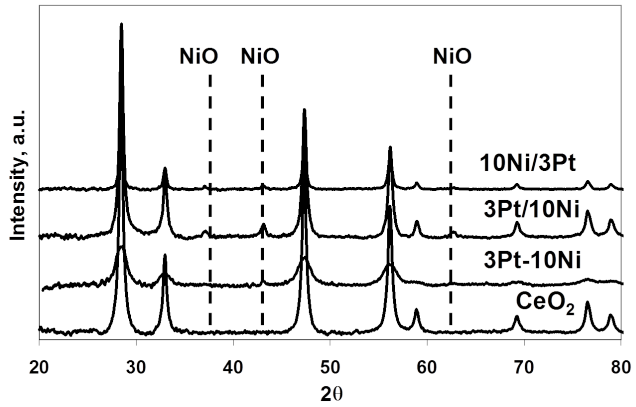

Figure 3: XRD patterns of PtNi-based catalysts and of CeO_2

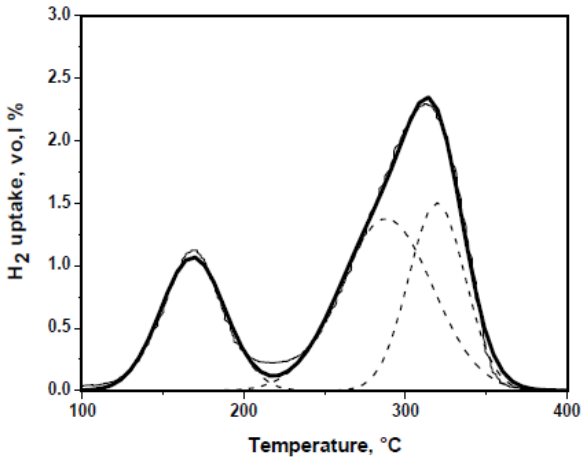

Figure 4: TPR profile of Pt / Ni catalyst after deconvolution

The XRD characterizations have also been done, in order to study both employed materials structure and crystallites dimension.

The XRD patterns of the unreduced bimetallic catalyst, based on both Pt and Ni, are presented in Fig. 3. They were compared with the XRD profile of the calcined CeO_2 and with the database of the International Centre for Diffraction Data (ICDD).

The peaks of the fluorite structure of the cerium oxide were detected in each case. The Ni-based catalysts also showed the peaks related to NiO (ICDD file: 78-0643, at 37.265°, 43.298° and 62.896°), probably formed during the calcination step. However, the comparison between the XRD spectra of the differently prepared catalysts showed less intense peaks for coprecipitated ones. For all the samples, no relevant peaks related to PtO_x species were detected probably due to the low metal load or to its high dispersion on the catalyst.

The crystallites sizes, calculated using the Scherrer formula (Eq. 2), are reported in Table 1; for NiO, the reference peak was located at 43.298° (1 1 0) while the crystallite dimensions of cerium oxide were obtained as the average between the values calculated for the peak at 28.542° (1, 1, 1), 47.475 (2, 2, 0) and 56.332 (3, 1, 1). The crystallites sizes are of the same order of magnitude (about 20 nm), except for the CeO_2 crystallites average dimension of the coprecipitated sample, which is 6...7 nm. This is in agreement with the lower intensity observed in the XRD profile.

The TPR profile, after deconvolution, for the 3 Pt / 10 Ni sample is reported in Fig. 4, showing that the reduction of catalysts occurred in two main temperature regions, the first, observed between 130 and 160°C, is assigned to the reduction of PtO_x species while the second wide bands at higher temperature could be associated with the reduction of the non-noble metal oxide [38, 41–44]. The same behavior is observed with 10Ni / 3Pt and 3Pt-10Ni sample, even if the second peak of the impregnated catalyst with the opposite impregnation order showed a wider and lower intensity. After deconvolution, it was possible to ascribe the contributions in a more precise way and to calculate the hydrogen uptake. The results are reported in Table 2. The experimental values were compared with the theoretical ones, obtained as a function of the metals load and of the expected metal oxides, taken from the literature. The reduction of PtO_2 to metallic Pt, using a catalyst containing 3wt% of platinum, involved 380 mmol H_2 / g_{cat}. Considering that the amount of non-noble metals was 10wt%, the hydrogen uptake related to the reduction of NiO to Ni

Table 2: TPR H_2 uptake of bimetallic Pt and Ni-based catalyst

Catalyst	T, °C	Experimental	Expected $Pt^{4+} \rightarrow Pt^0$	Expected $Ni^{2+} \rightarrow Ni^0$	Total experimental	Total expected
	168	480	287			
3Pt / 10Ni	288	856		1673	1984	1960
	319	649				
	159	335	277			
10Ni / 3Pt	287	853		1843	1602	2120
	323	414				
	206	327	328			
3Pt-0Ni	245	1463			3309	2188
	327	1058		1860		
	459	451				

was 1707 mmol H_2 / g_{cat}.

The samples showed a discrete agreement between the overall experimental hydrogen uptake and the expected value, with some differences in single contributions, probably due to spillover phenomena [45]. This kind of behavior can be particularly amplified in the case of coprecipitated catalysts, which showed an experimental hydrogen uptake considerably higher than the theoretical one; beside this, this discrepancy could also be due to the low dimensions of the crystallites, which gives higher reducibility to the catalyst.

3.2. Catalytic tests in diluted conditions

The tests in diluted feed stream were performed in fixed operating conditions: P = 1 atm, T = 300°C, GHSV = 15,000 h^{-1}, Q_{TOT} = 1,000 Ncm^3 / min. The feed mixture had the following composition: 0.5 vol% EtOH / 1.5 vol% H_2O / 98 vol% N_2, hence the dilution ratio was 49 and the water-to-ethanol molar ratio 3 (r.d.=49, r.a.=3). All tests were carried out at GHSV = 15,000h^{-1} for a reaction time of about 60 min.

The bimetallic catalysts results, shown in terms of X_{EtOH}, Y_{H2} and S_p, are reported in Tables 3 and 4 and compared with the values obtained for the monometallic samples.

The monometallic platinum-based catalysts showed a very interesting performance, but the formation of acetone as by-product reduced hydrogen yields. In the presence of these samples, in fact, dehydrogenation of ethanol to acetaldehyde, followed by the decarbonylation of acetaldehyde to acetone occurs. However, by increasing the metal load in the range 1...5, selectivity towards hydrogen and carbon dioxide increases; in particular, with 5 wt% Pt / CeO_2, the reformate gas mainly contains CH_4, CO_2 and H_2, since the ability of the system to minimize CO and C_3H_6O formation is higher.

Table 3: Ethanol and water conversion and hydrogen yield in ESR on CeO_2 supported monometallic and bimetallic. Experimental conditions: T = 300°C, EtOH = 0.5vol%, EtOH:H_2O:N_2 = 0.5:1.5:98, Total gas flow rate = 1000 Ncm^3 / min, GHSV = 15,000 h^{-1}, Time on stream = 1 h

Catalyst	X_{EtOH}, %	Y_{H2}, %
1Pt	90	30
3Pt	100	37
5Pt	100	38
10Ni	89	25
20Ni	80	23
1Pt / 10Ni	100	43
1Pt / 20Ni	100	42
3Pt / 10Ni	100	45

Taking into account the significant activity of nickel in steam reforming reactions and its lower cost with respect to noble metals, it was also used as active phase in monometallic cerium oxide-supported samples. The nickel-based catalysts performed worse than the platinum-based samples. In particular, ethanol conversion was lower than 90% and undesired acetaldehyde was also detected in the products distribution. However, by varying the nickel amount in the range 10...20wt%, it is possible to observe the highest

Table 4: Product selectivities in ESR on CeO_2 supported monometallic and bimetallic. Experimental conditions: T = 300°C, EtOH = 0.5vol%, EtOH:H_2O:N_2 = 0.5:1.5:98, Total gas flow rate = 1000 Ncm^3 / min, GHSV = 15,000 h^{-1}, Time on stream = 1 h

Catalysts	S_{CH4}, %	S_{CO}, %	S_{CO2}, %	S_{H2}, %	S_{C2H4}, %	S_{C3H6O}, %	S_{C2H4O}, %
1Pt	31	21	26	30	0	16	0
3Pt	43	2	56	39	0	1	0
5Pt	40	0	59	38	0	0	0
10Ni	17	20	8	28	0.2	9	7
20Ni	19	19	10	28	0.2	0	0
1Pt / 10Ni	35	0.1	56	44	0.1	0	0
1Pt / 20Ni	34	0.5	55	42	0	0	0
3Pt / 10Ni	50	1	56	44	0	0	0

hydrogen yield and ethanol conversion on 10% Ni / CeO_2.

Some bimetallic samples, containing Pt and Ni, and supported on CeO_2 were investigated, with the idea being to combine the properties of noble and non-noble metals by using a platinum load lower than 5wt%. It is evident that the formation of undesired products can be avoided through the combination of a non-noble metal with a small amount of noble metal, since any acetaldehyde, acetone and ethylene trace is recorded for the Pt / Ni samples. When nickel is already deposited on cerium oxide, the addition of a small amount of platinum (1wt%) is able to considerably raise the ethanol conversion and hydrogen yield, lowering, at the same time, CO levels in the products mixture. It was confirmed that the optimal nickel load is 10 wt%, while it is not necessary to reach 5wt% of platinum, like in the monometallic sample. 3 Pt / 10 Ni / CeO_2 gives a very interesting performance, ensuring total ethanol conversion. The maximum value of hydrogen selectivity is obtained, likely thanks to the aptitude of platinum to enhance the hydrogenation capability of nickel. Moreover, scarce carbon monoxide selectivity was noticed and there was an absence of undesired by-products. In fact, the carbon mass balance closure was verified, when calculated considering CH_4, CO and CO_2 as C-containing products in the outlet stream.

The effect of temperature was also investigated, in the range 300...450°C, for 3Pt / 10Ni. The results are reported in Fig. 5, where the reactants conversion and hydrogen yield are shown as a function of temperature while in Fig. 6 the product selectivities are presented as a function of temperature. Ethanol conversion is total in the temperature range examined while water conversion reaches 63% at 450°C; the hydrogen yield increases 10% passing from 300 to 450°C. Moreover, at T≥450°, the values remain stable. Concerning the production of carbon-containing products, methane selectivity decreases from

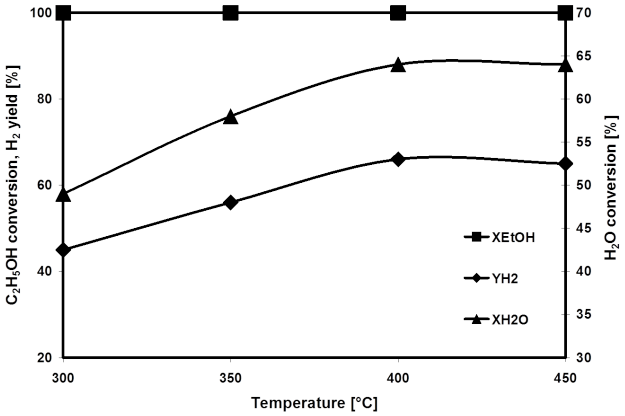

Figure 5: Effect of temperature on ethanol and water conversion and on hydrogen yield in ESR on CeO_2 supported Pt / Ni catalysts. Experimental conditions: EtOH = 0.5 vol%, EtOH : H_2O : N_2 = 0.5 : 1.5 : 98, Total gas flow rate = 1,000 Ncm^3 / min, GHSV = 15,000 h^{-1}, Time on stream = 1 h

50 to 24% by increasing temperature from 300 to 450°C and, simultaneously, CO_2 one varies from 44 to 65%. However, despite the considerable values of H_2 yield (higher than 50% at 450°C), the growth in CO selectivity from 0 to 9% must be taken into account.

The bimetallic catalyst is capable of achieving very interesting performances, as it showed total ethanol conversion, high hydrogen yield and no by-product formation at very low temperatures. In contrast, in the case of the monometallic samples, higher temperatures were required to achieve complete ethanol conversions.

3.3. Catalytic tests in concentrated conditions

3Pt / 10Ni catalyst was also tested in more concentrated conditions, in order to better simulate the real amount of ethanol present in the raw bio-ethanol stream.

A total flow rate of 1,000 Ncm^3 / min was used, at the following feed stream composition: 5% C_2H_5OH / 15%

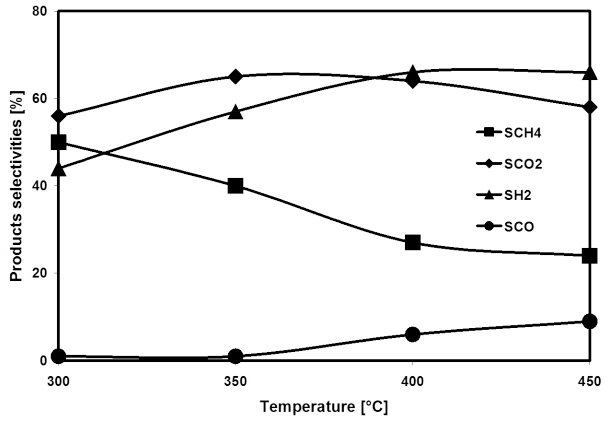

Figure 6: Effect of temperature on products selectivities in ESR on CeO_2 supported Pt / Ni catalyst. Experimental conditions: EtOH = 0.5 vol%, EtOH:H_2O:N_2 = 0.5:1.5:98, Total gas flow rate = 1000 Ncm^3 / min, GHSV = 15,000 h^{-1}, Time on stream = 1 h

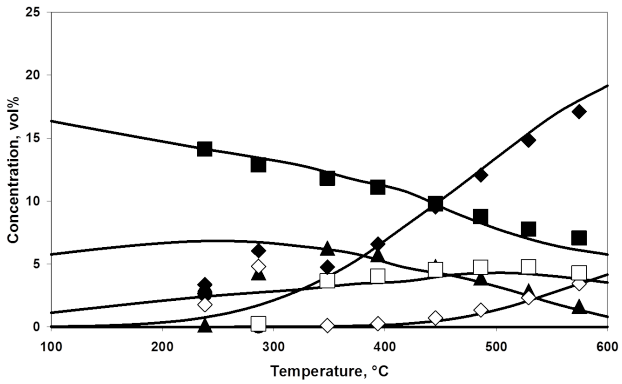

Figure 7: Experimental (points: filled square H_2O, filled diamond H_2, filled triangle CH_4, open square CO_2, open diamond CO, filled circle C_2H_5OH) and equilibrium (lines) products' distribution as a function of temperature for 3Pt / 10Ni in concentrated catalytic tests (total flow rate = 1000 Ncm^3 / min; GHSV = 15,000 h^{-1}; r.d. = 4; r.a. = 3)

H_2O / 80% N_2 (corresponding to r.d. = 4; r.a. = 3), the GHSV was fixed at 15,000h^{-1} and the temperature range was 300...600°C.

In Fig. 7 the products distribution measured at the reactor outlet after the LT-ESR reaction is shown in comparison with the equilibrium calculations. The sample performance is very interesting, also in concentrated conditions: besides complete ethanol conversion, even at low temperatures, there is very good agreement with the thermodynamic predictions, even at low contact times.

The presence of platinum appears crucial for the desired reaction, allowing more promising behavior than the monometallic sample, with higher conversion toward the desired products.

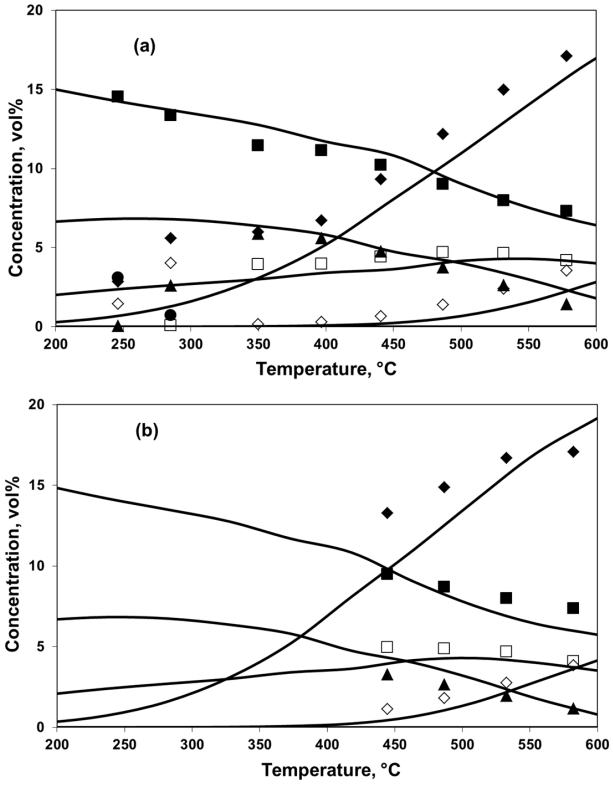

Figure 8: Experimental (points: filled square H_2O, filled diamond H_2, filled triangle CH_4, open square CO_2, open diamond CO, filled circle C_2H_5OH) and equilibrium (lines) products' distribution as a function of temperature for 10 Ni / 3 Pt (a) and 3 Pt-10 Ni (b) in concentrated catalytic tests (total flow rate = 1,000 Ncm^3 / min; GHSV = 15,000 h^{-1}; r.d. = 4; r.a. = 3)

In particular, in the range 330...480°C methane is the main product and this aspect makes the Pt / Ni catalyst very useful when LT-ESR is proposed as a pre-reforming step before the MSR reaction [46].

The catalyst 10Ni / 3Pt, prepared by impregnation but with a reverse order, was also used for LT-ESR in concentrated conditions. With respect to 3Pt / 10Ni, worse agreement between the products distribution and the equilibrium distribution was observed (Fig. 8a), in particular at low temperature, where ethanol was not completely converted. This was probably related to the deposition of nickel on platinum: the poor availability of a noble metal on the catalyst surface disadvantages the conversion of reactants.

The coprecipitated 3Pt-10Ni catalyst, despite the highest reducibility, was characterized by no significant activity for the desired reaction, as reported in Fig. 8b. In fact, a strong disagreement with the thermodynamic previsions was observed and lower hydrogen yield were obtained.

As a consequence, the results of this first activity screen-

ing lead to a preliminary conclusion that the catalysts prepared by impregnation are more suitable for the ESR reaction. In particular, adding the noble metal last ensures higher performances. Therefore, as 3Pt / 10Ni seemed the most promising candidate for the LT-ESR reaction, the effect on its catalytic properties of other macroscopic parameters was studied.

The feed stream was further concentrated, using dilution ratios of 1.5 and 0.67, corresponding to the following feed stream compositions: 10%C_2H_5OH / 30%H_2O / 60%N_2 and 15%C_2H_5OH / 45%H_2O / 40%N_2.

As expected, in both cases, the sample performance was negatively affected by the decrease in the dilution ratio, since worse agreement with the thermodynamic calculations was observed and the ethanol was not completely converted at low temperatures. Nevertheless, at temperatures higher than 450°C, the 3Pt / 10Ni sample appears attractive again, ensuring total ethanol conversion and no considerable change in the C-containing products. In fact, the Pt / Ni sample appears highly active and selective for the desired reaction in the investigated operating conditions.

The effect of the GHSV was also studied (here not reported), finding that, predictably, lower values lead to stronger agreement between the experimental and the equilibrium products distribution, even at very low temperatures. In particular, at 7500 h^{-1} ethanol was totally converted at r.d.<4 and T<450°C.

Moreover, the Pt / Ni performances were investigated in terms of stability, monitoring the activity and selectivity of the catalyst as a function of reaction time, during LT-ESR. The operating conditions of the Time-on-stream (TOS) test were: T = 450°C, P = 1 atm, GHSV = 15,000 h^{-1}, total flow rate = 1000 Ncm^3 / min with r.d. = 1.5 (10vol% of ethanol) and r.a. = 3.

The results, reported in Fig. 9, are shown in terms of the products concentration profile as a function of reaction time. All the concentrations were almost stable, suggesting high stability of the catalyst, However, after about 300 min, the TOS was stopped because a significant increase occurred in the pressure drops. This behavior was related to reactor plugging, which typically accompanies sintering or coke phenomena. Since the mass balance was close to 99% and no evidence of gaseous by-products was detected from FT-IR spectra related to the outlet stream, the catalysts after the TOS test were further characterized to better understand the reactor plugging. The crystallites sizes were calculated using the Scherrer formula from the XRD pattern of the Pt / Ni sample after the stability test and compared with the ones calculated for the fresh catalyst: the values were very close to each other, thus sintering phenomena were considered absent or not appreciable. N_2 adsorption experiments were repeated on the 3Pt / 10Ni after the TOS test and a higher SSA value was measured (40 m^2 / g for the fresh sample vs 60 m^2 / g for the treated catalyst). This result suggests the formation of carbonaceous substances on the catalyst surface.

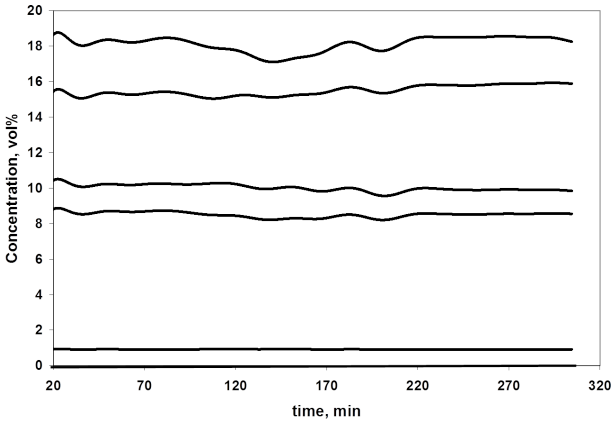

Figure 9: Product concentration profile as a function of reaction time during the stability test. (Total flow rate = 1000 Ncm^3 / min; GHSV = 15,000 h^{-1}; r.d. = 4; r.a. = 3) for Pt / Ni sample

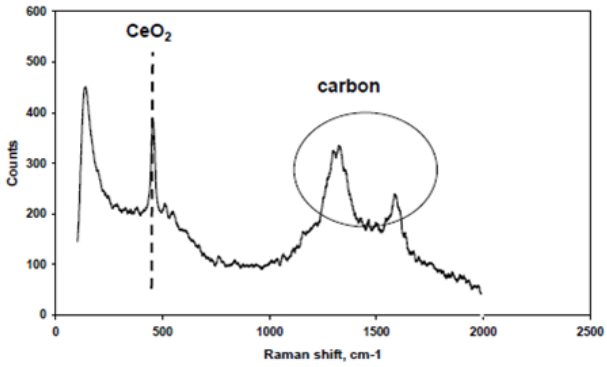

Figure 10: Raman spectrum after stability test for Pt / Ni catalyst

This hypothesis became certainty after the TG-MS analysis and Raman spectrum interpretation. Submitting the sample to a flow of air at 10°C / min from room temperature to 800°C, a weight loss of about 3.4% was calculated in the range 400...600°C, correlated to the CO_2 mass fragment (m / z = 44). Moreover, the typical signals of carbonaceous species were detected at a Raman shift of about 1590 cm^{-1} [47–49], as reported in Figure 10; the CeO_2 presence was also evident at about 460 cm^{-1}.

This result is very peculiar, ensuring closure of the carbon mass balance even without considering any by-products. In reality, the carbon deposited on the Pt / Ni surface was

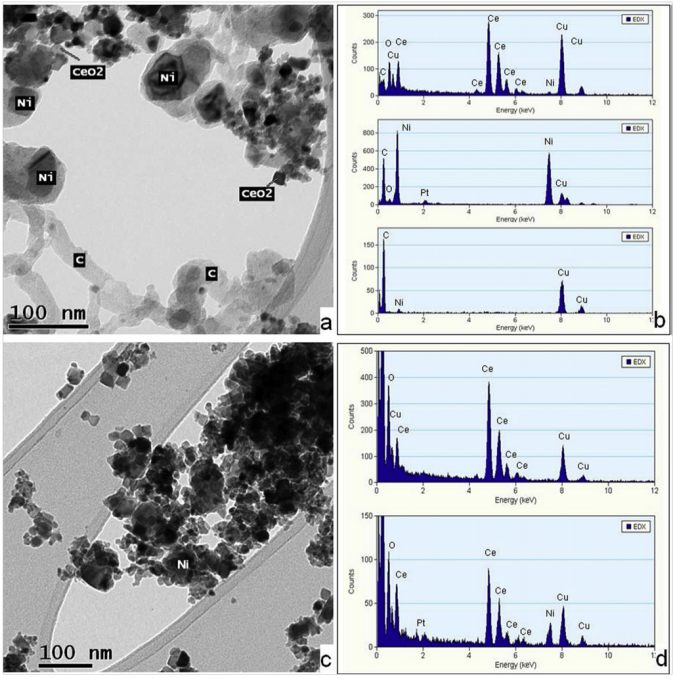

Figure 11: TEM image and EDS spectra ((a) and (c) respectively) of Pt / Ni sample after TOS test (Total flow rate = 1000 Ncm^3 / min; GHSV = 15,000 h^{-1}; 10 vol.% EtOH; T = 450°C); TEM image and EDS spectra ((b) and (d) respectively) of Pt / Ni sample before ESR reaction and after TPR (5 vol.% H_2 / N_2; heating rate: 10°C / min up to 600°C). For interpretation of the color references in this figure legend, the reader is referred to the web version of this article

quantified, discovering that it is less than 1% of the carbon fed as ethanol. Therefore coke selectivity is too low to be detected from balances and, consequently, to cause the deactivation of the catalyst.

In Fig. 11, TEM-EDS observations of the 3Pt / 10Ni catalyst after the TOS test (Fig. 11a and c) and before the ESR test (Fig. 11b and d) were compared.

TEM analysis of the exhaust sample showed ceria nanocrystalline aggregates, Ni particles and amorphous carbonaceous filaments, also observed in the related EDX spectra (CeO_2 (top), Ni (middle) and carbonaceous filaments (bottom)) reported in Fig. 11c. In contrast, from TEM-EDS observations of the sample after TPR measurements (i.e. before the ESR test) no evidence of carbon was detected and only a small number of CeO_2 and NiO grains were present. In Fig. 11d, the EDX spectrum of one of the grains of ceria (top) and of an aggregate of different grains (bottom) were compared. The more intense Ni peak observed in the latter case revealed that part of the grains in the TEM image are Ni species.

These latter characterization results show the linkage between Pt signal and Ni particles, leading to the hypothesis of the formation of a platinum-nickel solid solution. The analysis of TPR profiles, described in Section 3.1, gave further validation to this assumption: the stronger interaction between Pt and Ni oxides results in the higher reducibility of Pt species in the Pt / Ni sample with respect to the one prepared by impregnation with a reverse order. By abstracting, it is easy to relate the hypothesis of a solid solution to the better performance of the 3Pt / 10Ni / CeO_2 catalyst.

The stability of the 3Pt / 10Ni sample was also tested with a higher water-to-ethanol molar ratio, using an r.a. value of 6. A considerable increase in 3Pt / 10Ni stability was observed: comparing the time required to reach a limit value of pressure drops (about 1 bar) in the case of r.a. = 3 and r.a. = 6, it is interesting to note the capacity of water to enhance the durability of the system from 300 to 700 min. Also in this case, all the characterization techniques were performed on the catalyst after the stability test, observing, for instance, no SSA increase with respect to the fresh catalyst. This leads to the conclusion that water is very helpful, since it favors the gasification of the coke deposited on the catalyst surface or, as reported in some papers, has a specified role to play in avoiding carbon formation.

4. Conclusions

The LT-ESR reaction is here proposed as a competitive method to produce hydrogen, using a clean, renewable feedstock combined with well-established technology. It is also proposed to carry out the ESR reaction at temperatures lower than 600°C, in order to reduce the thermal duty and CO formation.

The catalytic aspects of LT-ESR were evaluated, through the performances of bimetallic catalysts, based on Pt and Ni. The activity, selectivity and stability of the samples were compared with the behavior of the correspondent monometallic catalysts, with the same non-noble metal load. Various characterization techniques were helpful in better understanding properties of the samples.

The activity of each catalyst was studied in a diluted feed, to realize a first screening, and in more concentrated conditions, to evaluate the effect of the main macroscopic parameters on the performance of the catalysts.

3Pt / 10Ni / CeO_2 appears more promising than the equivalent monometallic samples in the same circumstances, especially in terms of activity and selectivity towards the desired product, due to the presence of Pt at the gas-solid interface promoting ethanol adsorption and hydrogenation of CH_x coke precursors [16, 41]. It was also more suitable

than the catalyst prepared with reverse impregnation order and the coprecipitated one.

The 3Pt / 10Ni sample enabled high methane selectivity to be achieved, even at low contact time and at a stoichiometric water-to-ethanol molar ratio. Its stability is affected by coke formation phenomena, typical of nickel-based catalysts, which can be avoided by using more water in the feed stream. This is not an added cost, in terms of the energy requirement linked to water vaporization, since in the real bio-ethanol stream the amount of water is considerably higher than the stoichiometric one (in the range 13...20, depending on the biomass) [12].

Acknowledgements

The authors thank Tecnimont for financial assistance.

References

[1] X. Zhai, S. Ding, Z. Liu, Y. Jin, Y. Cheng, Catalytic performance of ni catalysts for steam reforming of methane at high space velocity, international journal of hydrogen energy 36 (1) (2011) 482–489.

[2] C.-H. Wang, K.-F. Ho, J. Y. Chiou, C.-L. Lee, S.-Y. Yang, C.-T. Yeh, C.-B. Wang, Oxidative steam reforming of ethanol over ptru/zro 2 catalysts modified with sodium and magnesium, Catalysis Communications 12 (10) (2011) 854–858.

[3] H.-S. Roh, I.-H. Eum, D.-W. Jeong, Low temperature steam reforming of methane over ni–ce (1- x) zr (x) o 2 catalysts under severe conditions, Renewable Energy 42 (2012) 212–216.

[4] J. Xu, G. F. Froment, Methane steam reforming: Ii. diffusional limitations and reactor simulation, AIChE Journal 35 (1) (1989) 97–103.

[5] M. Abashar, Coupling of steam and dry reforming of methane in catalytic fluidized bed membrane reactors, International Journal of Hydrogen Energy 29 (8) (2004) 799–808.

[6] H.-W. Kim, K.-M. Kang, H.-Y. Kwak, J. H. Kim, Preparation of supported ni catalysts on various metal oxides with core/shell structures and their tests for the steam reforming of methane, Chemical Engineering Journal 168 (2) (2011) 775–783.

[7] S.-K. Ryi, J.-S. Park, D.-K. Kim, T.-H. Kim, S.-H. Kim, Methane steam reforming with a novel catalytic nickel membrane for effective hydrogen production, Journal of Membrane Science 339 (1) (2009) 189–194.

[8] P. Udani, P. Gunawardana, H. C. Lee, D. H. Kim, Steam reforming and oxidative steam reforming of methanol over cuo–ceo 2 catalysts, international journal of hydrogen energy 34 (18) (2009) 7648–7655.

[9] A. Basagiannis, X. Verykios, Catalytic steam reforming of acetic acid for hydrogen production, International Journal of Hydrogen Energy 32 (15) (2007) 3343–3355.

[10] K. Takeishi, H. Suzuki, Steam reforming of dimethyl ether, Applied Catalysis A: General 260 (1) (2004) 111–117.

[11] B. S. Kwak, J. Kim, M. Kang, Hydrogen production from ethanol steam reforming over core–shell structured nixoy–, fexoy–, and coxoy–pd catalysts, International Journal of Hydrogen Energy 35 (21) (2010) 11829–11843.

[12] A. Demirbas, Biofuels sources, biofuel policy, biofuel economy and global biofuel projections, Energy conversion and management 49 (8) (2008) 2106–2116.

[13] M. Li, S. Li, C. Zhang, S. Wang, X. Ma, J. Gong, Ethanol steam reforming over ni/ni x mg 1- x o: Inhibition of surface nickel species diffusion into the bulk, international journal of hydrogen energy 36 (1) (2011) 326–332.

[14] D. K. Liguras, K. Goundani, X. E. Verykios, Production of hydrogen for fuel cells by catalytic partial oxidation of ethanol over structured ni catalysts, Journal of Power Sources 130 (1) (2004) 30–37.

[15] K. Vasudeva, N. Mitra, P. Umasankar, S. Dhingra, Steam reforming of ethanol for hydrogen production: thermodynamic analysis, International Journal of Hydrogen Energy 21 (1) (1996) 13–18.

[16] A. L. Alberton, M. M. Souza, M. Schmal, Carbon formation and its influence on ethanol steam reforming over ni/al 2 o 3 catalysts, Catalysis Today 123 (1) (2007) 257–264.

[17] C. Rossi, C. Alonso, O. Antunes, R. Guirardello, L. Cardozo-Filho, Thermodynamic analysis of steam reforming of ethanol and glycerine for hydrogen production, International Journal of Hydrogen Energy 34 (1) (2009) 323–332.

[18] A. Erdőhelyi, J. Raskó, T. Kecskés, M. Tóth, M. Dömök, K. Baán, Hydrogen formation in ethanol reforming on supported noble metal catalysts, Catalysis Today 116 (3) (2006) 367–376.

[19] L. Hernández, V. Kafarov, Thermodynamic evaluation of hydrogen production for fuel cells by using bio-ethanol steam reforming: Effect of carrier gas addition, Journal of Power Sources 192 (1) (2009) 195–199.

[20] J. L. Silveira, L. B. Braga, A. C. C. de Souza, J. S. Antunes, R. Zanzi, The benefits of ethanol use for hydrogen production in urban transportation, Renewable and Sustainable Energy Reviews 13 (9) (2009) 2525–2534.

[21] H.-S. Roh, A. Platon, Y. Wang, D. L. King, Catalyst deactivation and regeneration in low temperature ethanol steam reforming with rh/ceo2–zro2 catalysts, Catalysis Letters 110 (1-2) (2006) 1–6.

[22] H.-S. Roh, Y. Wang, D. L. King, A. Platon, Y.-H. Chin, Low temperature and h2 selective catalysts for ethanol steam reforming, Catalysis letters 108 (1-2) (2006) 15–19.

[23] A. Boyano, A. Blanco-Marigorta, T. Morosuk, G. Tsatsaronis, Exergoenvironmental analysis of a steam methane reforming process for hydrogen production, Energy 36 (4) (2011) 2202–2214.

[24] D. P. Harrison, Z. Peng, Low-carbon monoxide hydrogen by sorption-enhanced reaction, International Journal of Chemical Reactor Engineering 1 (1).

[25] E. Aneggi, M. Boaro, C. de Leitenburg, G. Dolcetti, A. Trovarelli, Insights into the redox properties of ceria-based oxides and their implications in catalysis, Journal of Alloys and Compounds 408 (2006) 1096–1102.

[26] H. Song, U. S. Ozkan, Changing the oxygen mobility in co/ceria catalysts by ca incorporation: Implications for ethanol steam reforming†, The Journal of Physical Chemistry A 114 (11) (2009) 3796–3801.

[27] J. Llorca, N. Homs, J. Sales, P. R. de la Piscina, Efficient production of hydrogen over supported cobalt catalysts from ethanol steam reforming, Journal of Catalysis 209 (2) (2002) 306–317.

[28] F. Aupretre, C. Descorme, D. Duprez, D. Casanave, D. Uzio, Ethanol steam reforming over mg x ni 1- x al 2 o 3 spinel oxide-supported rh catalysts, Journal of Catalysis 233 (2) (2005) 464–477.

[29] A. C. Basagiannis, P. Panagiotopoulou, X. E. Verykios, Low temperature steam reforming of ethanol over supported noble metal catalysts, Topics in catalysis 51 (1-4) (2008) 2–12.

[30] T. Yamazaki, N. Kikuchi, M. Katoh, T. Hirose, H. Saito, T. Yoshikawa, M. Wada, Behavior of steam reforming reaction for bio-ethanol over pt/zro 2 catalysts, Applied Catalysis B: Environmental 99 (1) (2010) 81–88.

[31] A. N. Fatsikostas, D. I. Kondarides, X. E. Verykios, Production of hydrogen for fuel cells by reformation of biomass-derived ethanol, Catalysis Today 75 (1) (2002) 145–155.

[32] J. Sun, X.-P. Qiu, F. Wu, W.-T. Zhu, H2 from steam reforming of ethanol at low temperature over ni/y2o3, ni/la2o3 and ni/al2o3 catalysts for fuel-cell application, International Journal of Hydrogen Energy 30 (4) (2005) 437–445.

[33] M. Benito, R. Padilla, J. Sanz, L. Daza, Thermodynamic analysis and performance of a 1kw bioethanol processor for a pemfc operation, Journal of power sources 169 (1) (2007) 123–130.

[34] F. Mariño, G. Baronetti, M. Jobbagy, M. Laborde, Cu-ni-k/γ-al 2 o 3 supported catalysts for ethanol steam reforming: formation of hydrotalcite-type compounds as a result of metal–support interaction, Applied Catalysis A: General 238 (1) (2003) 41–54.

[35] A. C. Furtado, C. G. Alonso, M. P. Cantao, N. R. C. Fernandes-Machado, Bimetallic catalysts performance during ethanol steam reforming: influence of support materials, international journal of hydrogen energy 34 (17) (2009) 7189–7196.

[36] A. Vizcaíno, A. Carrero, J. Calles, Ethanol steam reforming on mg-and ca-modified cu–ni/sba-15 catalysts, Catalysis Today 146 (1) (2009) 63–70.

[37] Y. Men, G. Kolb, R. Zapf, V. Hessel, H. Löwe, Ethanol steam reforming in a microchannel reactor, Process safety and environmental protection 85 (5) (2007) 413–418.

[38] G. Jacobs, R. A. Keogh, B. H. Davis, Steam reforming of ethanol over pt/ceria with co-fed hydrogen, Journal of Catalysis 245 (2) (2007) 326–337.

[39] A. Ruggiero, Hydrogen production by low temperature reforming of bio-ethanol, Ph.D. thesis, University of Salerno (2009).

[40] B. Banach, A. Machocki, P. Rybak, A. Denis, W. Grzegorczyk, W. Gac, Selective production of hydrogen by steam reforming of bio-ethanol, Catalysis Today 176 (1) (2011) 28–35.

[41] P. Ciambelli, V. Palma, A. Ruggiero, Low temperature catalytic steam reforming of ethanol. 1. the effect of the support on the activity and stability of pt catalysts, Applied Catalysis B: Environmental 96 (1) (2010) 18–27.

[42] E. Heracleous, A. Lee, K. Wilson, A. Lemonidou, Investigation of ni-based alumina-supported catalysts for the oxidative dehydrogenation of ethane to ethylene: structural characterization and reactivity studies, Journal of Catalysis 231 (1) (2005) 159–171.

[43] D. Das, T. N. Veziroglu, Hydrogen production by biological processes: a survey of literature, International Journal of Hydrogen Energy 26 (1) (2001) 13–28.

[44] T. Paryjczak, J. Rynkowski, S. Karski, Thermoprogrammed reduction of cobalt oxide catalysts, Journal of Chromatography A 188 (1) (1980) 254–256.

[45] C. de Leitenburg, A. Trovarelli, J. Kašpar, A temperature-programmed and transient kinetic study of co 2 activation and methanation over ceo 2 supported noble metals, Journal of Catalysis 166 (1) (1997) 98–107.

[46] S. S.-Y. Lin, H. Daimon, S. Y. Ha, Co/ceo 2-zro 2 catalysts prepared by impregnation and coprecipitation for ethanol steam reforming, Applied Catalysis A: General 366 (2) (2009) 252–261.

[47] R. McCabe, C. Wong, H. Woo, The passivating oxidation of platinum, Journal of Catalysis 114 (2) (1988) 354–367.

[48] A. E. Galetti, M. F. Gomez, L. A. Arrua, M. C. Abello, Ethanol steam reforming over ni/znal 2 o 4-ceo 2. influence of calcination atmosphere and nature of catalytic precursor, Applied Catalysis A: General 408 (1) (2011) 78–86.

[49] W. Wang, Y. Wang, Steam reforming of ethanol to hydrogen over nickel metal catalysts, International Journal of Energy Research 34 (14) (2010) 1285–1290.